Available online at www.sciencedirect.com
SCIENCE DIRECT®
Catalysis Today 89 (2004) 159–167
CATALYSIS TODAY
www.elsevier.com/locate/cattod

Recombination of oxygen atomic excited states produced by non-equilibrium RF plasma on different semiconductor materials: catalytic phenomena and modelling

C. Guyon*, S. Cavadias, I. Mabille, M. Moscosa-Santillan, J. Amouroux

Laboratoire de Génie des Procédés Plasmas ENSCP, 11 rue Pierre et Marie Curie, Paris 75005, France

Abstract

The purpose of this work is the study of oxygen atoms recombination on type n or p oxide semiconductors with various gap energies. The oxygen atoms are produced by a non-equilibrium low pressure RF plasma tubular reactor. The pressure is between 100 and 200 Pa. The relative oxygen atom concentration and the recombination coefficient (γ) were measured by actinometric optical emission spectroscopy (AOES). A plot of the γ coefficient versus $1/T$ allows the determination of the activation energy recombination. The results for p-type semiconductors show an increase of the activation energy with the gap energy. The recombination coefficient increases as gap energy decreases. In the case of n-type semiconductors, the activation energy depends on the number of active sites. Hence, the recombination of oxygen atoms depends on the electronic properties of the oxide semiconductors. The simulation of recombination of oxygen atoms on the oxide semiconductors was performed with a kinetic model of 18 reaction including three gas–surface reactions, using the Chemkin® Surface code. The calculated values of the recombination coefficient show a good agreement with the experimental results in the temperature range of 300–900 K and give a good prediction up to 1200 K.

Keywords: Plasma; Catalycity; Recombination; Oxygen; Oxide semiconductors; Chemkin®

1. Introduction

When atoms strike the surface of a material they may recombine to form molecules. The ratio of recombined atoms over the number of the atoms striking the surface (γ coefficient) depends on the nature and the temperature of the material.

The energy released during atom recombination is shared between the resulting molecules and the surface. The sharing of this energy (β coefficient) depends on the nature of the material and the process of recombination (Eley–Rideal or Langmuir–Hinshelwood) through the residence time of the atoms in the surface and the activation energy. However, as oxygen atoms have very high sticking coefficients, an oxide layer is formed in the surface in a few milliseconds, leading to the modification of the nature of the surface and its properties [1–8]. This process is very important for the design of catalysts on material supporting high thermal constraints [9]. In previous works [10–12], it was pointed out that the n-type semiconductors as SiO_2, ZnO, WO_3 and Fe_2O_3 have lower catalycity than p-type semiconductors as Co_3O_4, Ag_2O and CuO_2. Moreover, the lower the energy gap of forbidden band, the higher the catalycity is.

In this paper new experimental results on Fe_3O_4 and CVD-SiC are compared to our previous experimental results on CoO, MnO, PbO, Sb_2O_3, WO_3, $BaTiO_3$, TiO_2, $CaTiO_3$, Al_2O_3 and SiC/SiO_2 [11–13] in the temperature range from 300 to 773 K. Also, we present models for the prediction of the catalycity of the semiconductors, in the case Eley–Rideal mechanism, as well as the formation and recombination of oxygen atoms using Chemkin®. The principle of recombination coefficient measurement and the actinometric method is described in Section 2. The experimental set-up used for these measurements is described in Section 3. Section 4 contains the results and their interpretation while in Section 5 the prediction of the catalycity of the semiconductors is presented. The model for the simulation of oxygen atoms recombination on silica using Chemkin® is presented in Section 6. Finally, Section 7 is a brief conclusion on the fitting of the model and the experimental results.

* Corresponding author.

0920-5861/$ – see front matter © 2003 Elsevier B.V. All rights reserved.
doi:10.1016/j.cattod.2003.11.022

2. Recombination coefficient measurement—actinometric method

Considering the recombination of oxygen atoms on a surface as a first order kinetics, the flux of recombined atoms N is:

$$N = k_w[O]_g \tag{1}$$

where $[O]_g$ is the concentration of oxygen atoms in gas phase (atoms m^{-3}) and k_w is defined as the constant factor by which the gas-phase density of atoms at the surface must be multiplied to obtain the surface rate of conversion of atoms into molecules per unit area and unit time ($m\,s^{-1}$). The catalytic behaviour of a gas–surface system may be expressed in terms of recombination probability γ, defined as the ratio *flux of atoms recombined on the surface/flux of atoms impinging on the surface* $= N/Z$.

In a purely diffusion regime the flux of atoms impinging a surface is:

$$Z = [O]_g\sqrt{\frac{kT}{2\pi m_O}} \tag{2}$$

where m_O is the mass of an oxygen atom (kg) and T the surface temperature (K).

Combining (1) and (2), the recombination coefficient ($\gamma = N/Z$) becomes

$$\gamma = k_w\sqrt{\frac{2\pi m_O}{kT}} \tag{3}$$

known as the *Hertz–Knudsen* relation. The reaction constant k_w can be written as [14]:

$$k_w = C_a\frac{kT}{h}\frac{f^*}{f_a F_g}\exp\left(-\frac{E_a}{RT}\right) \tag{4}$$

where E_a is the activation energy for the recombination ($J\,mol^{-1}$), C_a the concentration of oxygen atoms adsorbed on the active sites (atoms m^{-2}) and f^*, f_a, F_g are partition functions of the activated complex, the activated species and the gas-phase atoms, respectively.

As [14]

$$\frac{f^*}{f_a} \cong 1 \tag{5}$$

and

$$F_g = \left(\frac{2\pi m_O kT}{h^2}\right)^{3/2} \tag{6}$$

thus

$$k_w = C_a\frac{h^2}{(2\pi m_O)^{3/2}(kT)^{1/2}}\exp\left(-\frac{E_a}{RT}\right) \tag{7}$$

By replacing (7) into (3), a relation between γ and the activation energy E_a of the recombination is obtained:

$$\gamma = \frac{C_a h^2}{2\pi m_O kT}\exp\left(-\frac{E_a}{RT}\right) \tag{8}$$

Putting,

$$T_O = \frac{C_a h^2}{2\pi m_O k} \tag{9}$$

the relation (8) becomes:

$$\gamma = \frac{T_O}{T}\exp\left(-\frac{E_a}{RT}\right) \tag{10}$$

So, if the recombination coefficient γ is known at different temperatures, the activation energy of the process and the number of the active sites can be deduced by plotting $\ln(\gamma T)$ versus $1/T$.

The recombination coefficients are determined using the actinometric optical emission spectroscopy(AOES) [15]. In this non-perturbing in-situ method, a small amount of non-reactive gas (e.g. argon) allows the emission intensities to be correlated with relative ground state concentrations. In our case, the ground state of O atoms concentration has been monitored with optical emission from O (844.6 nm) and Ar (811.5 nm). The ratio I_O/I_{Ar} obtained by actinometry is related to the concentration ratio by $I_O/I_{Ar} = k(O)/(Ar)$ [16], and it can be used as a tracer for atomic oxygen concentration.

The validity of the actinometry method has been verified by titration of the atomic oxygen with nitric oxide. As the number of O atoms hitting the surface is derived from kinetic theory, the assumption is made that the regime is purely diffusional without any convection. That means that AOES is valid at low pressures (100–200 Pa). Under these conditions, the recombination coefficient γ, can be calculated from the atomic oxygen concentration profile along the reactor:

$$\gamma = \frac{-4D\nabla(I_O/I_A)_x}{c(-\nabla(I_O/I_A)_x L + (I_O/I_A)_0)} \tag{11}$$

where D is the binary diffusion coefficient ($m^2\,s^{-1}$), L the width of the boundary layer (m), $\nabla(I_O/I_{Ar})_x$ the axial gradient of concentration ratio and $(I_O/I_{Ar})_0$ the steady state ratio.

3. Experimental set-up

The experimental set-up consists of a plasma tubular reactor, supplied with a control and acquisition device (Fig. 1). All experiments are performed at 110 Pa pressure, with a flow of 400 sccm air (N_2/O_2), and 25 sccm argon (about 5% of the total gas flow). The plasma is created by a 13.56 MHz generator. The discharge is pulsed 2 s "on" and 5 s "off" in order to avoid the heating of the surface by the plasma itself. The emission spectroscopy signal is transmitted via an optical fibre and analysed by a monochromator with an optical multichannel analyser (OMA) detector.

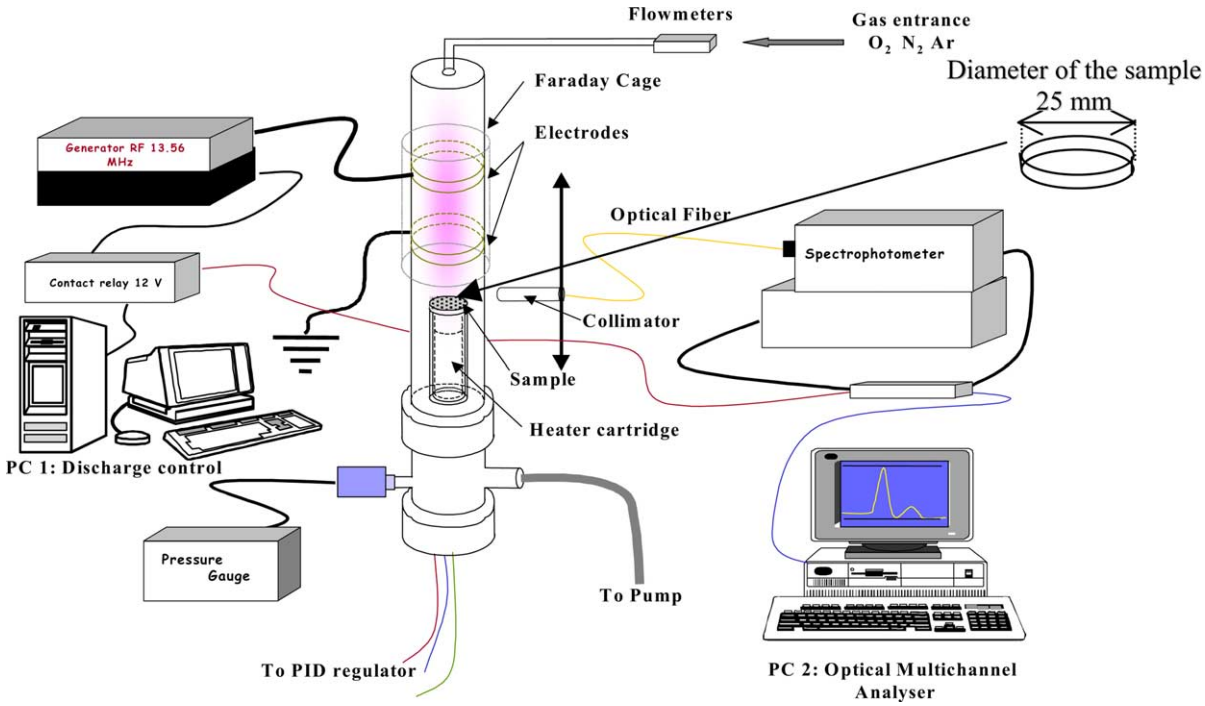

Fig. 1. Experimental set-up for the recombination coefficient measurement in pulsed discharge.

4. Determination of recombination coefficient γ and activation energy E_a

The recombination coefficient of atomic oxygen on each sample has been measured in a temperature range from 300 to 923 K. The gap energy of the materials has been determined by optical reflection measurements [17] (Table 1).

For all the samples, an increasing of the recombination coefficient with their surface temperature can be noted.

The results for p-type semiconductors show an increase of the activation energy with the energy gap increase. Moreover, the lower the gap energy of the oxide is, the higher the recombination coefficient is. The electronic properties of the material influences strongly the heterogeneous recombination of the oxygen atoms. In the case of n-type semiconductors, the activation energy can be correlated to the number of active sites [11] (Table 1).

It was shown that the behaviour of p- or n-type oxide semiconductors is due to the adsorbed oxygen on the material [11,12,18]. Indeed for some samples a break of the slope is observed (Fig. 2). For example, in the case of WO_3, this change of slope occurs at about 600 K. At low temperature (300–600 K), the activation energy of the reaction can be estimated at $(4.3 \pm 0.7)\,\mathrm{kJ\,mol^{-1}}$. From 600 to 900 K, the activation energy is equal to $(12.9 \pm 2)\,\mathrm{kJ\,mol^{-1}}$. This difference between the activation energies can be explained

Table 1
Determination of the recombination coefficients of atomic oxygen on semiconductors and ceramic materials. Evolution with the surface temperature. Recombination activation energy of semiconductors

	Gap energy, E_{gap} (eV) (semiconductor type)	Recombination coefficient, γ (±20%) 300 K	Recombination coefficient, γ (±20%)	Activation energy, E_a (kJ mol^{-1}) (±15%) 300 K	Active sites, C_a (atoms m^{-2}) (±15%) 300 K	Activation energy, E_a (kJ mol^{-1}) (±15%) 773 K	Active sites, C_a (atoms m^{-2}) (±15%) 773 K
CoO	0.8 (p)	29×10^{-3}	34×10^{-3} (473 K)	4.1	2.3×10^{20}	4.1	2.3×10^{20}
MnO	1.3 (p)	17×10^{-3}	25×10^{-3} (473 K)	5.9	2.8×10^{20}	5.9	2.8×10^{20}
PbO	2.3 (p)	13×10^{-3}	18×10^{-3} (473 K)	6.4	3.0×10^{20}	6.4	3.0×10^{20}
Sb_2O_3	4.2 (p)	8.2×10^{-3}	21×10^{-3} (473 K)	9.9	6.3×10^{20}	9.9	6.3×10^{20}
Fe_3O_4	0.4 (n)	15×10^{-3}	28×10^{-3} (873 K)	6.9	3.3×10^{20}	6.9	3.3×10^{20}
WO_3	2.8 (n)	11×10^{-3}	24×10^{-3} (773 K)	4.3	1.1×10^{20}	12.9	7.3×10^{20}
$BaTiO_3$	3.1 (n)	12×10^{-3}	78×10^{-3} (773 K)	5.2	1.6×10^{20}	23.4	79×10^{20}
TiO_2	3.1 (n)	14×10^{-3}	31×10^{-3} (773 K)	5.4	2.5×10^{20}	5.4	2.5×10^{20}
$CaTiO_3$	3.5 (n)	13×10^{-3}	28×10^{-3} (773 K)	5.8	2.0×10^{20}	19.6	25×10^{20}
Al_2O_3	7.3 (n)	9.7×10^{-3}	61×10^{-3} (773 K)	10.3	8.1×10^{20}	10.3	8.1×10^{20}
CVD-SiC	11 (n)	3×10^{-3}	30×10^{-3} (773 K)	11.8	3.4×10^{20}	29.6	78.8×10^{20}
SiC/SiO_2	11 (n)	4×10^{-3}	9.3×10^{-3} (773 K)	7	1.1×10^{20}	74 (973 K)	–

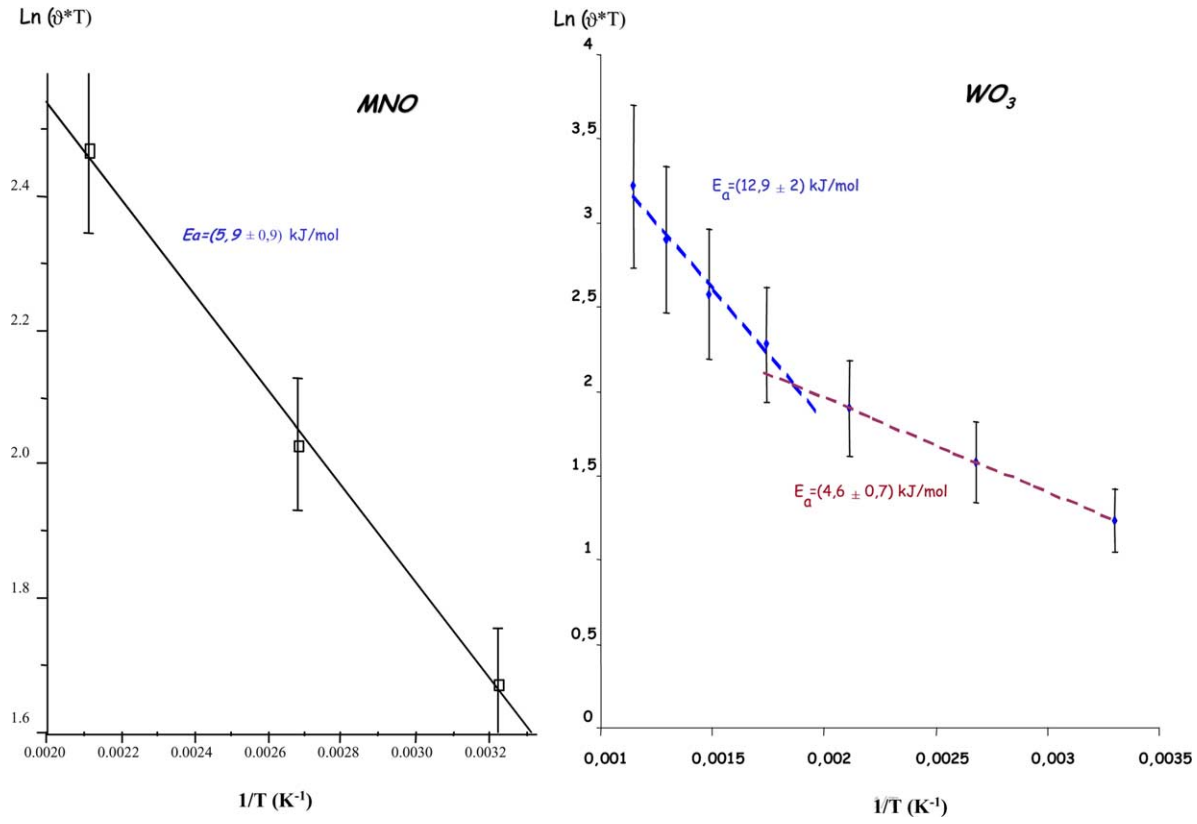

Fig. 2. Evolution of the recombination coefficient with the surface temperature. Determination of the activation energies for a MnO and WO_3 samples: $D(O_2) = 50\,\text{sccm}\,\text{min}^{-1}$, $D(N_2) = 200\,\text{sccm}\,\text{min}^{-1}$, $D(Ar) = 15\,\text{sccm}\,\text{min}^{-1}$, pressure = 110 Pa, power of the RF = 240 W, and discharge time of 2000 ms.

as an evolution of the recombination mechanism. At low temperature, the recombination reaction is controlled by an Eley–Rideal mechanism whereas at high temperature, by a Langmuir–Hinshelwood mechanism. Furthermore, in a previous work, it has been shown that the change in the reaction mechanism is not due to the diffusion of oxygen [14]. The same behaviour has been observed for other n-type semiconductors as SiO_2, $BaTiO_3$ and $CaTiO_3$.

5. Evaluation of the activation energies for n- and p-type semiconductors

In order to show the dependence of the activation energy previously on the gap energy of p-type semiconductors and on the active sites concentration for the n-type ones, a model was developed.

The hypotheses of the model are:

- oxygen is adsorbed on the semiconductor preferentially under the form O^-;
- the recombination take place according to the Eley–Rideal mechanism.

During the adsorption step, an oxygen atom is adsorbed on a hole $V_O{}^+$ getting an electron from the conduction band (I). The adsorbed atom recombines with an oxygen atom from the gas phase and the formed molecule desorbs immediately (II):

$$\text{(I)}\quad V_O^+ + e_{BC}^- + O_g \underset{k_{des}}{\overset{k_{ads}}{\Leftrightarrow}} O_{ads}^-,$$

$$\text{(II)}\quad O_g + O_{ads}^- \overset{k_{II}}{\Rightarrow} O_{2g} + V_O^+ + e_{BC}^-$$

with

$$k_{ads} = \frac{S_O}{(1 - S_O/2)} \frac{1}{[V_O^+]_0^\tau} \sqrt{\frac{kT}{2\pi m_O}} \tag{12}$$

$$k_{des} = \nu\, e^{-E_{des}/RT} \tag{13}$$

and,

$$k_{II} = k_{II}^0\, e^{-E_a/RT} \tag{14}$$

where S_O is the sticking coefficient without adsorbed oxygen, $[V_O^+]_0$ the total density of the adsorption sites (m^{-2}), m_O the mass of an oxygen atom (kg), τ the sum of stoichiometric coefficients (=1 for the adsorption), ν the vibration frequency of O_{ads}-surface (s^{-1}), E_a the activation energy of the recombination process ($J\,mol^{-1}$), E_{des} the desorption energy of oxygen atom ($J\,mol^{-1}$), k_{adss} the adsorption rate constant (s^{-1}), k_{des} the desorption rate constant (s^{-1}), O_{ads}^- the density of adsorbed atoms (m^{-2}) and O_g the density of gas-phase atoms (m^{-3}).

Applying the steady state approximation for the adsorbed O^-_{ads} species, we have:

$$\frac{d[O^-_{ads}]}{dt} = 0 = k_{ads}[V^+_O][e^-_{BC}][O_g] - k_{des}[O^-_{ads}] - k_{II}[O_g][O^-_{ads}] \quad (15)$$

considering that $[V^+_O] = [V^+_O]_0 - C_a$, $[O^-_{ads}] = C_a$, $[e^-_{BC}] = n_c V$ and $[O_g] = C_g$. Thus, the reaction rate constant k_{II} becomes

$$k_{II} = V k_{ads}\left(\frac{V^+_O}{C_a} - 1\right) n_c - \frac{k_{des}}{C_g} \quad (16)$$

where V is the volume of the treated material (m^3), C_a the surface density of occupied adsorption sites (site m^{-2}), C_g the volume density of oxygen atoms in the gas phase, e^-_{BC} the electronic density in the conduction band (m^{-2}) and n_c the electron density in the conduction band (m^3).

And k_{II} depends on the electronic density in the conduction band n_c. This last parameter can be evaluated if [19]:

- the Fermi level is located out of the valence and conduction band on the impurity levels (donors or acceptors);
- the behaviour of the semiconductor is controlled by the impurities extrinsic semiconductors type n or p, that means $|N_d - N_a| \gg n_i$.

Where N_d is the volumetric density of donor impurities (atoms m^{-3}), N_a the volumetric density of acceptor impurities (atoms m^{-3}) and n_i the electronic density of the conduction band at temperature T for an intrinsic semiconductor (without impurities), defined by

$$n_i^2(T) = n_c(T)\,p_v(T) = \frac{1}{16}\left(\frac{\pi kT}{2h^2}\right)^3 (m_c m_v)^{3/2}\, e^{(-E_{gap}/kT)} \quad (17)$$

m_v is the effective mass of holes (kg) and m_c the effective mass of electrons (kg).

In the case of an n-type semiconductor ($N_d > N_a$) : $n_c(T) = N_d - N_a$ while for a p-type one is ($N_a > N_d$):

$$n_c(T) \cong \frac{n_i^2(T)}{N_d - N_a} \quad (18)$$

Also, the recombination constant k_{II} for n-type is given by the following expression:

$$k_{II} = V k_{ads}\left(\frac{[V^+_O]_0 - 1}{C_a}\right)(N_d - N_a) - \frac{k_{des}}{C_g} \quad (19)$$

and for a p-type semiconductor

$$k_{II} = \frac{V}{16} k_{ads}\left(\frac{[V^+_O]_0}{C_a} - 1\right)\left(\frac{\pi kT}{2h^2}\right)^3 (m_c m_v)^{3/2} \exp\left(-\frac{E_{gap}}{kT}\right) - \frac{k_{des}}{C_g} \quad (20)$$

An examination of these recombination constants indicates clearly that in the case of a n-type semiconductor the activation energy is independent of the gap energy as for a p-type semiconductor the activation energy increases with a rise in the gap energy. Nevertheless, this model cannot explain the better catalycity of p-type semiconductor. Probably, this is because the influence of the electrostatic repulsion in the adsorption rate for n-type ones has not been taken into account.

The activation energies for these two types of semiconductors can be deduced from (19) and (20) by simplifying the k_{des}/C_g term, because the desorption is not the limiting step for the recombination. Also between 300 and 500 K, we can consider the coverage of the surface equal to 0.5 for any material: $C_a/[V^+_O]_0 = 0.5$ and $m_c = m_v = m_e$, the effective mass of electrons. After these simplifications, the activation energies for n- and p-type semiconductors are calculated from relations (21) and (22), respectively.

n-type:

$$E_a = -RT \ln\left[V\frac{k_{ads}([V^+_O]_0)}{k^0_{rec}}(N_d - N_a)\right] \quad (21)$$

p-type:

$$E_a = E_{gap}\frac{R}{k} - RT \ln \times \left[\frac{V}{16}\frac{k_{ads}([V^+_O]_0)}{k^0_{rec}}\left(\frac{\pi kT}{2h^2}\right)^3 \frac{m_e^3}{(N_a - N_d)}\right] \quad (22)$$

The values of the parameters for the calculation of the activation energy are taken from the literature (E_{gap}, $|N_a - N_d|$) and experimental results. The density of donor and acceptor impurities in the materials and the recombination rate k^0_{II} were adjusted to fit with our experimental results.

The calculated values of E_a for p-type semiconductors at 300 K show a good agreement with the experimental measurements (Fig. 3). As it was expected, these energies increase with the gap energy (E_{gap}).

In case of n-type semiconductors we observe an increase of E_a with the density of active sites and a good agreement with the experimental results (Fig. 4). The deviation of the SiO_2 value may result from the fact that SiO_2 is obtained by an oxidation of SiC.

6. Simulation of the oxygen atom recombination on oxide semiconductors

In order to interpret the experimental results on a physical basis, we have developed a 18 reactions–15 species, kinetic model of oxygen atom recombination on oxide semiconductors (SiO_2). The 15 gas-phase reactions are issued from a detail gas-phase model not presented here [20]. It provides the evolution of the majors species (e^-, ions, radicals, atoms, etc.) occurring in an oxygen plasma. Three surface reactions have been added to this gas-phase model

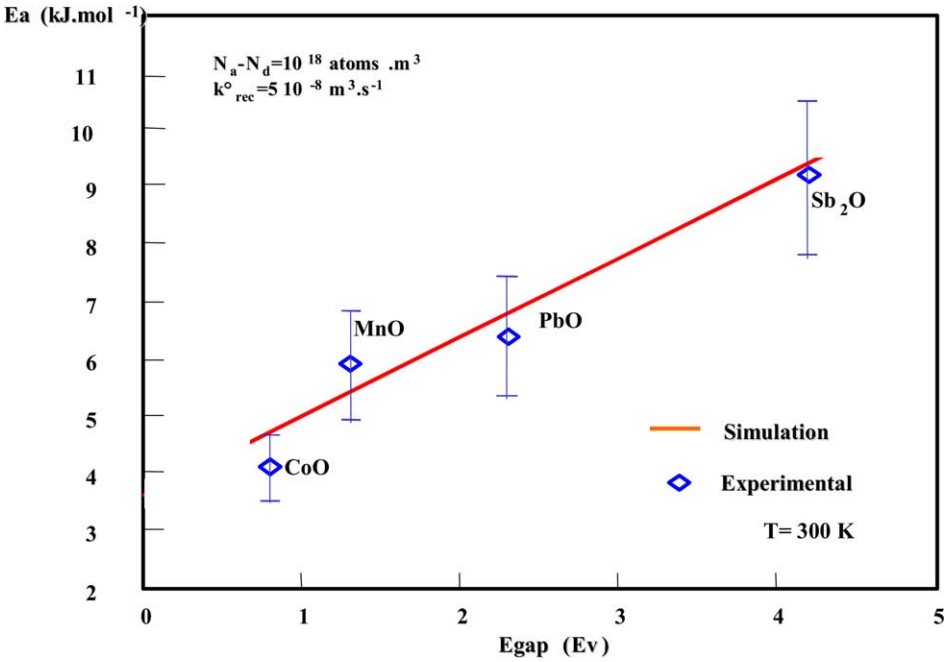

Fig. 3. Simulation of the activation energy of the recombination of O on the p-type semiconductors reaction vs. the energy gap.

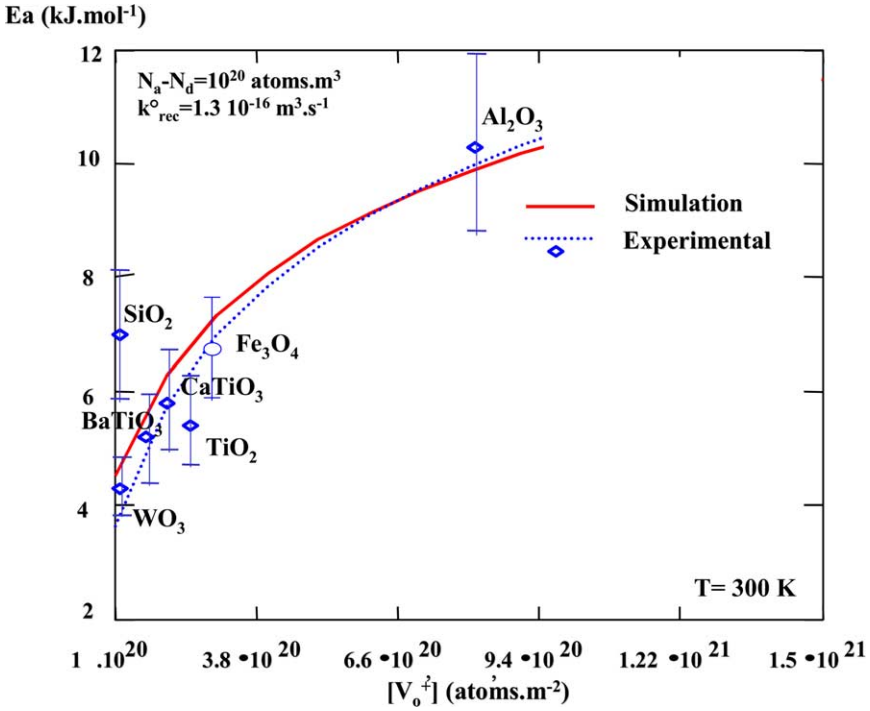

Fig. 4. Simulation of the activation energy of the recombination of O on n-type semiconductors reaction vs. the active sites density.

Table 2
Gas/surface reactions and reaction constants of atomic oxygen recombination on SiO_2

$O + Si_{(S)} \rightarrow Si\text{–}O_{ads}$ (a)	$k_a = 9 \times 10^9 \exp\left(\frac{-4096.6}{RT}\right)$ [24]	Adsorption
$O + Si\text{-}O_{ads} \rightarrow Si_{(S)} + O_2$ (b)	$k_b = 6 \times 10^{13} \exp\left(\frac{-954.6}{RT}\right)$	Recombination Eley–Rideal
$2Si\text{–}O_{ads} \rightarrow 2Si_{(S)} + O_2$ (c)	$k_c = 2 \times 10^{19} \exp\left(\frac{-2374.5}{RT}\right)$	Recombination Langmuir–Hinshelwood

(Table 2), in order to take into account the heterogeneous recombination of the oxygen atoms. Reaction (a) represents the adsorption step, while reactions (b) and (c) represent an Eley–Rideal recombination type [21–23] and a Langmuir–Hinshelwood recombination type [21,22,24], respectively. The reaction constants and activation energies for the 15 gas-phase reactions are taken from Hassouni [20] and for the oxygen adsorption (a) from Uda and Kato [23]. The simulation was performed using Chemkin® Surface. All calculations were made at 110 Pa, 250 W of the generator power and in a temperature range from 300 to 1200 K. Model parameters are: inlet flow rate, reactor volume and geometry as well as inlet composition. Special attention has been given to the gas–surface reactions and the determination of their activation energies (E_a) and kinetic constants (k_a, k_b, k_c).

The reaction constants were determined by the method of parameter estimation. In the reaction scheme of gas–surface interaction, kinetics for the three reactions depend on values of the Arrhenius parameters: the pre-exponential factor (A) and the activation energy (E_i). The more accurate these parameters, the closer the model will be to reality. As the activation energy was already evaluated, only the pre-exponential factor (A) was adjusted to fit the recombination coefficient (γ) measured experimentally.

The simulation of complete model (18 reactions, 15 species) was performed using the AURORA application of the Chemkin® code. This application can be applied to gas-phase stirred reactors and to systems that include surface reactions. In addition, it allows modelling of non-thermal plasma reactors taking into account ion and electron concentrations, the electron temperature as well as the neutral radical species concentrations. Well stirred reactors are characterised by constant reactor volume, mass flow rate, surface area, inlet composition and temperature, as well as the power induced into the plasma for non-thermal systems. Most of the contributing parameters were determined from the literature [21–27] and the experimental results.

Simulations were performed on SiO_2, Al_2O_3(n) and MnO(p). For the alumina and the manganese oxide, there is a good agreement up to 500 K (Fig. 5). However a deviation is observed for temperatures greater than 500 K. This deviation of simulated values from the experimental ones is due to the fact that our model deals only with the Eley–Rideal mechanism. So for temperatures higher than 500 K for MnO, there is probably a contribution of the Langmuir–Hinshelwood mechanism. In the case of SiO_2, a good agreement is observed between calculated values and experimental results of the recombination coefficients from 300 to 900 K (Fig. 6). An extrapolation of the results to higher temperature for γ coefficient predicts values of γ from 0.037 at 900 K to 0.088 at 1200 K These values are in agreement with those predicted by the Deutschmann's model.

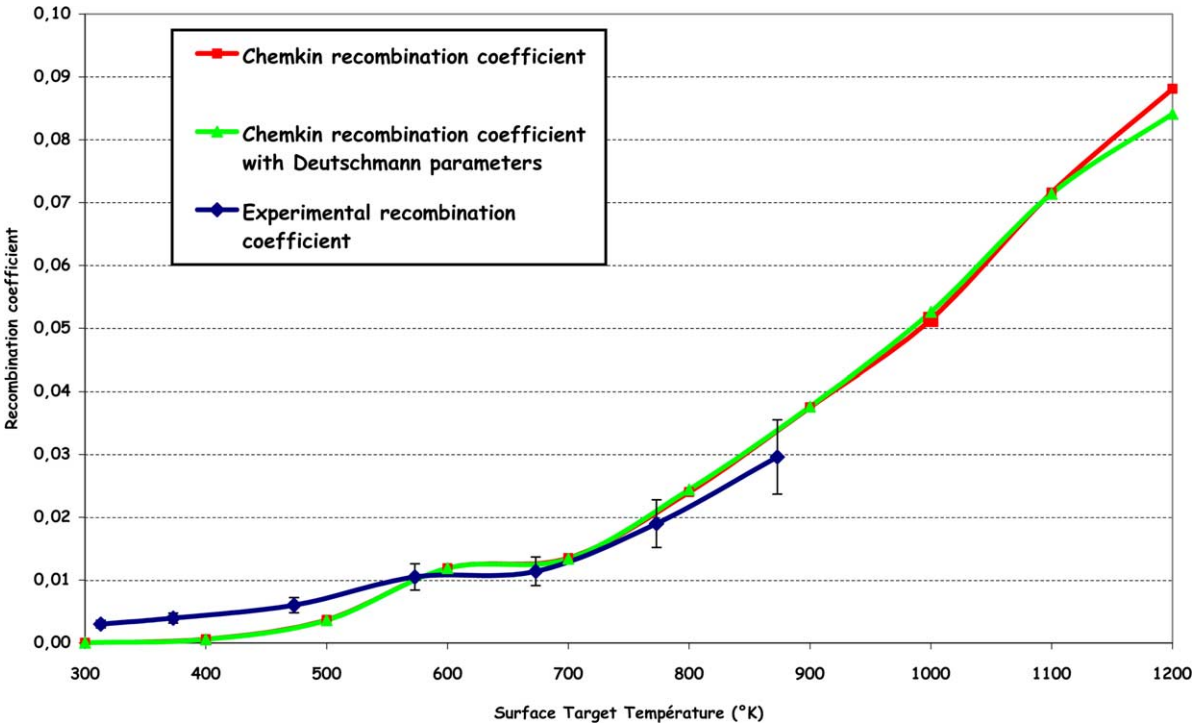

Fig. 5. Comparison between experimental and calculated recombination coefficients for silica: $D(O_2) = 50\,\text{sccm}\,\text{min}^{-1}$, $D(N_2) = 200\,\text{sccm}\,\text{min}^{-1}$, $D(Ar) = 15\,\text{sccm}\,\text{min}^{-1}$, pressure = 110 Pa, power of the RF = 240 W, and discharge time of 2000 ms.

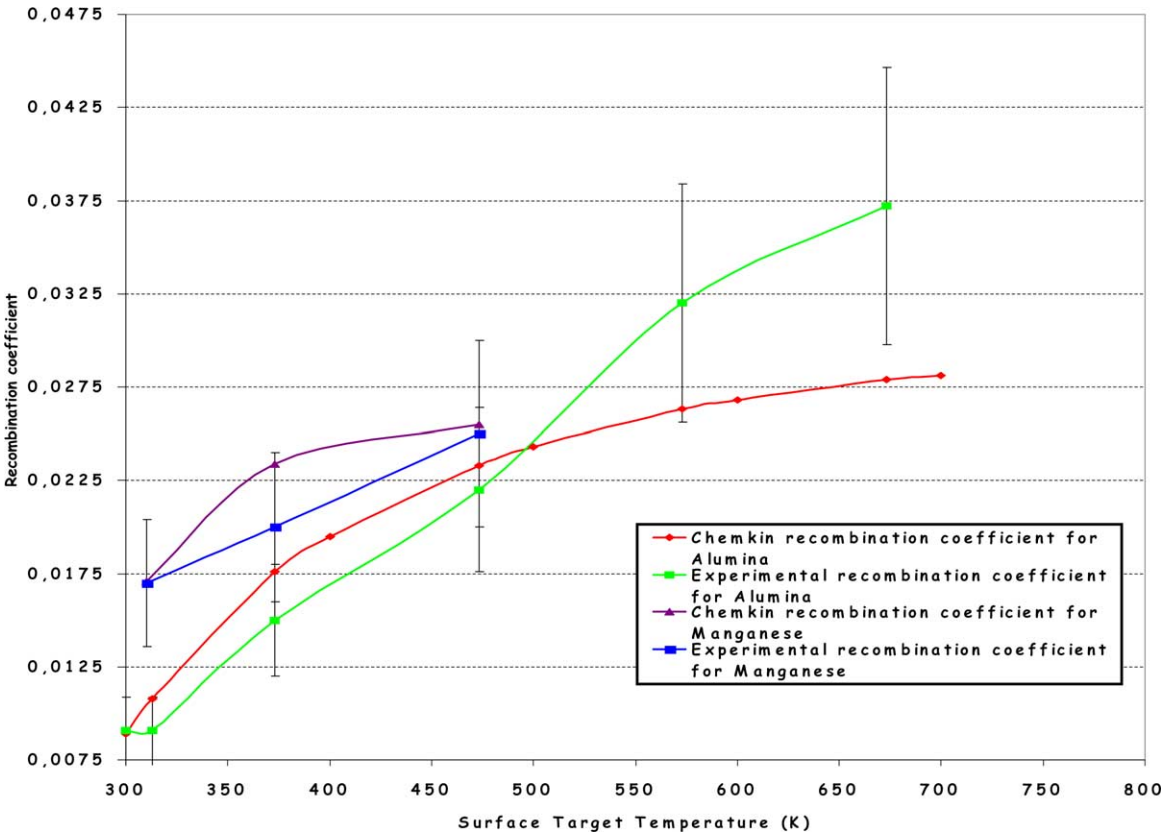

Fig. 6. Comparison between experimental and calculated recombination coefficients for alumina and manganese oxide: $D(O_2) = 50\,\text{sccm}\,\text{min}^{-1}$, $D(N_2) = 200\,\text{sccm}\,\text{min}^{-1}$, $D(Ar) = 15\,\text{sccm}\,\text{min}^{-1}$, pressure = 110 Pa, power of the RF = 240 W, and discharge time of 2000 ms.

7. Conclusion

The determination of γ coefficient, on metallic oxide semiconductors, leads to the determination of the role of the electronic properties of a material. The p-type semiconductors are more efficient to recombine the oxygen atoms than the n-type semiconductors. The electronic conduction of the material seems to have a great effect on the recombination efficiency. There is a correlation for p-type semiconductors between the activation energy and the gap energy. Likewise, the lower is the gap energy of the oxide, the higher is the recombination coefficient. For the n-type semiconductors the activation energy can be correlated to the density of active sites.

The use of AURORA, to modelling the recombination of oxygen atoms on oxides and ceramic surfaces, gives results in good agreement with the global recombination rate constants in the case of silica sample. These constants depend essentially on the temperature of the surface. Further development can be the implementation of the reaction mechanism in a CFD (computer fluid dynamics) code and the calculation of the heating for more complex surface shapes.

References

[1] R.H. Krech, J. Spacecraft Rockets 30 (1993) 509–513.
[2] F. Nguyen-Xuan, O. Mallard, S. Cavadias, J. Amouroux, A. Le Bozec, M. Rapuc, in: Proceedings of the Second European Symposium on Aerothermo-dynamics for Space Vehicles, Noordwijk, The Netherlands, 1994, pp. 457–461.
[3] G.A. Melin, R.J. Madix, Trans. Faraday Soc. 67 (1971) 198–211.
[4] A.L. Myerson, J. Chem. Phys. 50 (1969) 1228–1234.
[5] K. Nakada, Bull. Chem. Soc. Jpn. 32 (1959) 1072–1078.
[6] J.C. Greaves, J.W. Linnett, Trans. Faraday Soc. 54 (1958) 1323–1330.
[7] C.D. Scott, in: Proceedings of the AIAA Paper 80-1477, Snowmass, CO, 1980.
[8] E.V. Zoby, R.N. Gupta, A.L. Simmonds, in: Proceedings of the AIAA Paper 84-0224, Reno, NV, 1984.
[9] J. Warnatz, in: Proceedings of the 24th International Symposium on Combustion, Pittsburgh, 1992, pp. 553–579.
[10] C. Guyon, P. Cauquot, S. Cavadias, J. Amouroux, in: P. Fauchais (Ed.), Progress in Plasma Processing of Materials, Begell House, New York, 2001, pp. 101–108.
[11] C. Guyon, S. Cavadias, J. Amouroux, Surf. Coat. Technol. 142–144 (2001) 959–963.
[12] P. Cauquot, C. Guyon, S. Cavadias, J. Amouroux, in: Proceedings of the 14th International Symposium on Plasma Chemistry (ISPC 14), Praha, Czech Republic, 1999, pp. 127–132.
[13] P. Cauquot, S. Cavadias, J. Amouroux, High Temp. Mater. Process. 4 (2000) 365–378.
[14] K.J. Laidler, S. Glasstone, J. Eyring, J. Chem. Phys. 8 (1940) 659–676.
[15] D. Pagnon, J. Phys. D 2 (1995) 1856–1868.
[16] F. Nguyen-Xuan, Ph.D. Thesis, Pierre and Marie Curie University, France, 1997.
[17] J.I. Pankove, Optical Process in Semiconductors, Dover Publication, New York, 1975.

[18] P.B. Weisz, J. Chem. Phys. 20 (1952) 1483–1484.
[19] C. Kittel (Ed.), Introduction to Solid State Physics, 4th ed., Wiley, New York, 1971.
[20] K. Hassouni, Ph.D. Thesis, Pierre and Marie Curie University, France, 1992.
[21] C. Bruno, in: Proceedings of the US Air Force Academy, Colorado Springs, CO, 1989, P80840.
[22] O. Deutschmann, Coll, J. Heat Transfer 117 (1995) 495–501.
[23] T. Uda, K. Kato, in: Proceedings of the International Workshop on Challenges in Predictive Process Simulation, Wandlitz, Germany, 1997, pp. 17–20.
[24] W. Henry Weinberg, Acc. Chem. Res. 29 (10) (1996) 479–487.
[25] R.J. Willey, J. Thermophys. Heat Transfer 7 (1) (1993) 55–62.
[26] G. Cartry, L. Magne, G. Cernogora, J. Phys. D 32 (15) (1999) L53–L56.
[27] G. Cartry, L. Magne, G. Cernogora, J. Phys. D 33 (11) (2000) 1303–1314.